Applied Catalysis B: Environmental 236 (2018) 154–161

Contents lists available at ScienceDirect

Applied Catalysis B: Environmental

journal homepage: www.elsevier.com/locate/apcatb

A novel strategy to develop non-noble metal catalyst for CO_2 electroreduction: Hybridization of metal-organic polymer

Yeongdong Mun[a,1], Kyeounghak Kim[a,1], Seongbeen Kim[a], Seunghyun Lee[a], Seonggyu Lee[a], Sujeong Kim[a], Wonyong Choi[a,b], Soo-kil Kim[c], Jeong Woo Han[a,*], Jinwoo Lee[a,*]

[a] Department of Chemical Engineering, Pohang University of Science and Technology (POSTECH), Pohang, 37673, Republic of Korea
[b] Division of Environmental Science and Technology, Pohang University of Science and Technology (POSTECH), Pohang, 37673, Republic of Korea
[c] School of Integrative Engineering, Chungang University, Seoul, 06974, Republic of Korea

ARTICLE INFO

Keywords:
Electrocatalysts
CO_2 electroreduction
Non-precious metal catalysts
Organic-inorganic hybrid materials

ABSTRACT

Electrochemical CO_2 reduction reaction (CO_2RR) has attracted a lot of interest as a highly potential CO_2 utilization system. Due to the high overpotential in CO_2RR, an effective catalyst is required. We report a metal-organic hybrid catalyst (Co-PPy-C), which consists of Co and polypyrrole, as a highly active electrocatalyst for CO_2RR. Co-PPy-C exhibited high Faradaic efficiency and metal mass activity for CO production at low overpotential region. By density functional theory calculations, it was revealed that the catalytic site is the Co surface on which the deprotonated pyrrolic functionality in polypyrrole is adsorbed, and that the facile production of CO from CO_2 is due to the CO adsorption on the Co being weakened by the charge transfer from the Co surface to the polypyrrole. This work reports a new and active non-noble metal catalyst for CO_2RR, and provides the strategy of hybridization of metal and organic material to modify or enhance the catalytic activity of metal for CO_2RR.

1. Introduction

Currently, reducing the concentration of carbon dioxide (CO_2) in the atmosphere is an important environmental challenge. High concentration of atmospheric CO_2 has increased the greenhouse effect and may cause unpredictable climate changes, which threaten human life [1,2]. To reduce CO_2 emission effectively, new and renewable energy sources to replace fossil fuels, and technology to capture and use the emitted CO_2 should be developed simultaneously [3–5]. Electrochemical reduction of CO_2 is one of the promising strategy that converts CO_2 to valuable chemical species. The electrochemical reaction is highly advantageous because it can be conducted at ambient pressure and temperature, and can have high efficiency and simple operation unit [6–9].

Because the CO_2 reduction reaction (CO_2RR) is significantly dependent on catalysts, development of an effective electrochemical catalyst is of great importance to utilize CO_2 electroreduction as a practical strategy to utilize CO_2 [6,7,10]. Development of highly efficient CO_2RR catalyst must meet several requirements. 1) The catalyst for CO_2RR should have an appropriate adsorption energy for reaction intermediates of CO_2RR, to reduce the overpotential effectively. Generally, CO_2 is not easily activated on a catalyst that adsorbs CO_2 too weakly, but the catalyst can be poisoned if it adsorbs the reaction intermediates too strongly [11,12]. 2) The catalyst should have high selectivity for CO_2RR [13]. The hydrogen evolution reaction (HER) competes with CO_2RR in aqueous condition, so for CO_2RR, to be effective, the HER must be suppressed. 3) The reactions should yield chemicals that have high enough market value to repay the cost of the energy required for their production. Hydrocarbon production requires a large number of electrons per a molecule, so the production efficiency is relatively low and the production cost is typically high. However, CO and formic acid have high market value, considering the price of electricity, and consume only two electrons per one molecule during electrochemical production [14,15].

CO is a useful resource that can be converted to highly valuable chemicals by the FischerTropsch reaction or the Monsanto process [16–19]. Most catalysts that convert CO_2 to CO with high selectivity at low overpotential are expensive noble metals such as gold, silver, or palladium [17,20–23]. Some non-noble catalysts such as N-doped carbon or molybdenum disulfide can convert CO_2 to CO in electrolyte containing ionic liquid based on imidazolium [24,25], but such an electrolyte is generally too expensive to be used in large-scale electrochemical flow cells. To construct a practical electrochemical system for CO_2 utilization, a non-noble catalyst that has high catalytic activity for

* Corresponding authors.
E-mail addresses: jwhan@postech.ac.kr (J.W. Han), jinwoo03@postech.ac.kr (J. Lee).
[1] These authors contributed equally to this work.

https://doi.org/10.1016/j.apcatb.2018.05.025
Received 26 November 2017; Received in revised form 30 April 2018; Accepted 8 May 2018
Available online 09 May 2018
0926-3373/

CO_2RR in aqueous condition should be developed.

In this work, we discovered that extremely small cobalt (Co) nanoparticle hybridized with polypyrrole that was coated on conductive carbon black (Co-PPy-C) has high catalytic activity for CO production by CO_2RR in aqueous phase (in 0.1 M $KHCO_3$ solution). Co-PPy-C converted CO_2 to CO with high selectivity (CO Faradaic efficiency: 78%) at low overpotential region (at 0.55 V vs. RHE). Even if it has not been previously reported that Co nanoparticles or Co bulk metal converted CO_2 to CO electrochemically, the maximum metal (Co) mass activity of Co-PPy-C for CO production was as high as 91.3 mA mg_{Co}^{-1} at 0.7 V, which is one of the highest values among the metal particle catalysts for CO_2RR. Density functional theory (DFT) calculations suggested that this new catalytic behavior of Co metal for CO_2RR occurs because polypyrrole weakens the adsorption strength of CO on Co metal. It is known that CO is strongly adsorbed on a pure Co surface [26]. The adsorption property of a monometallic surface is highly dominated by a scaling relationship, which means that the adsorption energies of intermediates in the reaction change in the same direction [27]. Therefore, we infer that intermediates of CO_2RR are also strongly adsorbed on Co. This phenomenon can be advantageous for CO_2 activation, but it can poison the metal surface and deactivate it; this is well-known as the Sabatier principle [28]. Incorporation of polypyrrole on Co surface decreased its CO adsorption strength on Co surface, and resulted in the fast and selective CO production from CO_2 by facilitating CO desorption. This result is highly noteworthy in that the high catalytic activity for CO production by CO_2RR was achieved by hybridizing of non-noble metal and organic polymer, and shows the potential of metal/organic hybrid catalyst realistically that has been reported by the previous theoretical studies [29,30].

2. Experimental

2.1. Synthesis of Co-PPy-C

Composite material of Co and polypyrrole was synthesized by a two-step method composed of oxidative polymerization of pyrrole monomer and Co loading [31,32]. Vulcan XC-72 (0.5 g) was dispersed in ethanol (60 mL) by bath sonication. The solution was cooled down to 4 °C, then pyrrole monomer (0.1 mL) was added. Ammonium persulfate (APS) (48 mg) was dissolved in distilled water (35 mL). The APS solution was added dropwise to the pyrrole solution, then stirred for 12 h at 4 °C; the product (PPy-C) was collected by filtration and washing. PPy-C (98 mg) was dispersed in distilled water (50 mL) by bath sonication. Co nitrate hexahydrate (4.9 mg, $Co(NO_3)_2{\cdot}6H_2O$) was added to the solution. The solution was purged by N_2 bubbling, then heated to 80 °C. $NaBH_4$ (0.26 g) and NaOH (18.5 mg) were dissolved in distilled water (25 mL). The solution of $NaBH_4$ and NaOH was added dropwise to the solution containing PPy-C and $Co(NO_3)_2{\cdot}6H_2O$, and the mixture was held for 30 min at 80 °C; then the solution was cooled quickly to room temperature, filtered, and washed. Co-PPy-C was finally obtained. To obtain Co-PPy-2, 49 mg of $Co(NO_3)_2{\cdot}6H_2O$ and 90 mg of PPy-C were used to obtain Co-PPy-3, 147 mg of $Co(NO_3)_2{\cdot}6H_2O$ and 75 mg of PPy-C were used. To obtain Co-C, Co was directly loaded on Vulcan XC-72 without polypyrrole.

2.2. Electrochemical characterization and product analysis

The current collector on which the catalyst is loaded was made by coating carbon paper (Toray TGP-H-060, Toray Industries Inc.) with carbon black particles. Vulcan XC-72 (85 mg) and polytetrafluoroethylene binder (PTFE) (15 mg) were dispersed in 2-propanol (50 mL). The solution was sprayed on both sides of the carbon paper. The total loading amount of carbon black and binder was 1 mg cm^{-2} on each side. The coated carbon black was cut to be used as a current collector. The area except the active area was coated by epoxy resin to block the undesirable electrochemical reactions. To prepare catalyst slurry, the catalyst powder was sonicated in distilled water with Nafion® ionomer binder. The weight ratio of Nafion® ionomer to the catalyst was 0.5. The catalyst slurry was dropped to the active area of current collector by micropipette. The loading amount of catalyst was 1 mg cm^{-2}.

Electrolysis was conducted a glass electrochemical cell composed of two-compartments separated by an anion exchange membrane (Selemion AMV®, AGC, Japan). Ag/AgCl electrode was used as a reference electrode, and Pt mesh was used as a counter electrode. The electrolyte was 0.1 M $KHCO_3$ purged with CO_2, and the pH of the solution was 6.8. The working electrode was soaked in 7 mL of electrolyte in working part, and the electrolyte was replaced for each electrolysis. After purging CO_2 to the electrolyte for 20 min (10 mL min^{-1}), and the electrolysis was started by a potentiostat (Gamry Reference 600) with current interruption *iR* compensation mode. CO_2 was continuously supplied to the solution (10 mL min^{-1}). The product gas was injected automatically into a gas chromatography (GC, Agilent 7890B) by a six-port valve at the desired time (20 min after the start of electrolysis). H_2 and CO gas were detected by a thermal conductivity detector (TCD) and a flame ionization detector (FID) with a methanizer, respectively. GC peaks for each gas were calibrated using a customized reference gas mixture (RIGAS, Korea). We tried to detect the liquid product by using a Bruker Avance III Ascend 500, but no liquid product was detected. The Faradaic efficiencies and partial production currents were obtained by following equations.

For gas X,

$$FE_X = Q_X / Q_{total} \times 100 \quad (1)$$

$$Q_X = M_X \times e_X \times N_{Faradaic} \times \nu \quad (2)$$

$$Q_{total} = i_{injection} \quad (3)$$

$$i_X = i_{injection} \times FE_X \quad (4)$$

where FE_X (%) is the Faradaic efficiency for gas X, Q_X (C) is the consumed charge for production of gas X at the injection time, Q_{total} (C) is the total charge at the injection time, M_X is molar number of the injected gas X, e_X is the required number of electron for production of one X molecule, $N_{Faradaic}$ is Faradaic constant, ν is the flow rate of gas, $i_{injection}$ is the current at the injection time, i_X (A) is the partial production current for gas X.

2.3. Computational details

Density functional theory (DFT) calculations were performed using the Vienna ab initio Simulation Package (VASP) [33,34]. A (3 × 3) surface unit cell of Co(0001) with a vacuum thickness of 15 Å was used (Fig. S1) with the lattice constant of a = 2.507 Å and c = 4.069 Å, which is in good agreement with the experimental values of a = 2.507 Å and c = 4.070 Å. Considering the size of a unit of PPy chain (7.190 Å × 10.141 Å), the supercell size of Co(0001) was suitable to describe the PPy-Co model with the least mismatch of periodicity between Co surface and PPy chain. The exchange-correlation energies were treated using Perdew-Burke-Ernzerhof (PBE) functional based on a generalized gradient approximation (GGA) [35]. A planewave expansion with a cutoff of 400 eV was used with a 3 × 3 × 1 Monkhorst-Pack *k*-point sampling of the Brillouin zone [36]. Gaussian smearing was used with a width of 0.05 eV to determine the partial occupancies. We used the Methfessel-Paxton method with a width of 0.1 eV for the molecular adsorption on pure Co surface. The geometries were relaxed using a conjugate gradient algorithm until the forces on all unconstrained atoms were less than 0.03 eV $Å^{-1}$. In order to consider van der Waals interactions, we used DFT-D3 method suggested by Grimme [37].

The PPy and HPPy chain can be adsorbed on the Co (0001) surface with either vertical or parallel configuration. Previously, Lee et al. investigated HPPy-assisted oxygen reduction reaction (ORR) and oxygen

evolution reaction (OER) on $NdBa_{0.5}Sr_{0.5}Co_2O_{5+\delta}$ (NBSC) using vertical alignment model of HPPy on the NBSC surface [38]. In our system, however, we found that the parallel configuration of HPPy on Co(0001) is 1.05 eV more stable than the vertical configuration. For this reason, in this study we used the parallel configuration model of PPy-Co(0001) and HPPy-Co(0001).

The adsorption energy is defined as the total energy difference between before and after the molecular adsorption at each surface;

$$E_{ads} = E_{A^*} - E_{surf} - E_{A(g)}, \quad (5)$$

where E_{A^*} is the total energy of an adsorbate adsorbed on the surface and $E_{A(g)}$ is the total energy of an isolated molecule in the gas phase, and E_{surf} is the total energy of optimized clean surface structures. With this definition, a more negative value of E_{ads} indicates that the molecular adsorption is energetically favorable. The deprotonation reaction energy (E_R) of HPPy to PPy is defined as the total energy difference between before and after the dehydrogenation of HPPy.

$$E_R = E_{HPPy} - \left(E_{PPy} + 2E_{\frac{1}{2}H_2}\right), \quad (6)$$

where E_{HPPy} and E_{PPy} are the total energy of HPPy-Co(0001) and deprotonated PPy-Co(0001), respectively. $E_{\frac{1}{2}H_2}$ is the total energy of an isolated hydrogen molecule. With this definition, a negative reaction energy indicates the reduction of PPy is thermodynamically preferred. Since two hydrogen atoms are decomposed from HPPy to be PPy, we divided E_R by 2 to calculate $E_{R/Hatom}$.

To explore the change in charge distribution upon the introduction of HPPy and PPy onto Co(0001), we calculated charge density difference (Δρ) using the equations below;

$$\Delta\rho_{PPy-Co(0001)} = \rho_{PPy-Co(0001)} - \rho_{Co(0001)} - \rho_{PPy} \quad (7)$$

$$\Delta\rho_{HPPy-Co(0001)} = \rho_{HPPy-Co(0001)} - \rho_{Co(0001)} - \rho_{HPPy} \quad (8)$$

where $\rho_{PPy-Co(0001)}$ is the charge density of PPy-Co(0001), $\rho_{HPPy-Co(0001)}$ is the charge density of HPPy-Co(0001), $\rho_{Co(0001)}$ is the charge density of Co(0001), ρ_{PPy} is the charge density of PPy chain, and ρ_{HPPy} is the charge density of HPPy chain. The charge density was calculated with the frozen structures of Co(0001) surface, PPy chain and HPPy chain taken from the DFT-optimized structures of PPy-Co(0001) and HPPy-Co (0001).

For the case of charge transfer according to CO adsorption, $\rho_{PPy-Co(0001)}$, $\rho_{HPPy-Co(0001)}$, $\rho_{Co(0001)}$ are substituted to $\rho_{CO@PPy-Co(0001)}$, $\rho_{CO@HPPy-Co(0001)}$, $\rho_{CO@Co(0001)}$, respectively. $\rho_{CO@PPy-Co(0001)}$ is the charge density of CO adsorbed PPy-Co(0001) and ρ_{CO} is the charge density of CO molecule. The frozen structures of CO, PPy-Co(0001), and HPPy-Co (0001) taken from the DFT-optimized structures of CO adsorbed PPy-Co (0001) and HPPy-Co(0001) were also used to calculate charge density difference.

The amount of charge transferred from (H)PPy or Co(0001) to CO on (H)PPy-Co(0001) was calculated by the charge density difference between before and after the CO adsorption. The DFT-optimized structures of CO adsorbed PPy-Co(0001) and HPPy-Co(0001) were used to calculate the charge density difference.

3. Result and discussions

3.1. Material analysis

Co-PPy-C was synthesized by a simple two-step method in aqueous solution (Fig. 1a). Polypyrrole was coated on conductive carbon black (Vulcan XC-72, Cabot) by oxidative polymerization using APS as an oxidizing agent. Then Co was loaded on the polypyrrolecarbon black composite (PPy-C). A composite of polypyrrole and Co has been reported as a non-precious metal catalyst for the oxygen reduction reaction. Reductive catalytic activity for oxygen of the material has been studied since 2006 [32], but the catalytic property of the materials for CO_2RR has not been reported previously.

Transmission electron microscopy (TEM) image (Fig. 1b) and elemental mapping images obtained by electron energy loss spectroscopy (EELS) (Fig. 1c and 1d) show the distribution of each element in Co-PPy-C catalyst. The distribution of nitrogen (N) atoms (Fig. 1c) has the same shape as the TEM image of Co-PPy-C (Fig. 1b); this similarity means that polypyrrole was coated uniformly on the surface of carbon black particles. Co was also well distributed on PPy-C without aggregating into large particles (Fig. 1d). Thermogravimetric analysis (TGA) showed that loading of polypyrrole and Co was successful: when heated to 800 °C in N_2 atmosphere, PPy-C showed large weight change of 16 wt% due to the decomposition of polypyrrole, whereas carbon black (Vulcan XC-72) showed very small weight change (7 wt%) due to water evaporation and decomposition of oxygen functionalities from the carbon surface (Fig. S1a). The TGA result of Co-PPy-C obtained in air (Fig. S1b) showed that the amount of cobalt oxide that remained after thermal decomposition of carbonaceous material was 1.6%. Considering that the most stable cobalt oxide phase is Co_3O_4 at 800 °C (ambient pressure of air atmosphere) [39,40], the expected amount of Co in Co-PPy-C is 1.2 wt%, which is close to the result of inductive coupled plasma atomic emission spectroscopy (ICP-AES) (Co: 1.4%). As a comparison group, we synthesized additional catalyst composites with higher Co loadings than this, and named them Co-PPy-C-2 and Co-PPy-C-3. TGA results of Co-PPy-C-2 and Co-PPy-C-3 obtained in air also showed inorganic residue of 13.1% and 35.6% after heat-treatment (Fig. S1b), respectively; the amounts of Co on the catalysts obtained by TGA and ICP-AES analysis were summarized in Table S1.

There was no distinct peak in X-ray diffraction (XRD) pattern of Co-PPy-C except broad amorphous carbon peaks (near $2\theta = 25^\circ$ and 44°) due to the very low weight percent of Co (Fig. 2a). However, the XRD patterns of Co-PPy-C-2 and Co-PPy-C-3 showed clear peaks for Co_3O_4 and relatively much smaller peaks for CoO, so we infer that Co_3O_4 is the main Co species in the as-synthesized catalyst composites.

An elemental survey obtained by X-ray photoelectron spectroscopy (XPS) for Co-PPy-C also showed the presence of N and Co elements on the surface (Fig. 2b). Because of the polypyrrole coating on carbon black, the pyrrolic N functionality (399.5 ± 0.2 eV)[41] was observed solely in N 1s spectra obtained from both PPy-C and Co-PPy-C (Fig. 2c). This detection indicates that the pyrrolic functionality was not damaged by the process of loading Co. Weak Co $2p_{3/2}$ and $2p_{1/2}$ peaks were observed in Co 2p spectrum region; their positions were slightly shifted to the higher binding energy than the peaks obtained from commercial Co_3O_4 nanopowder (purchased from Sigma Aldrich) (Fig. 2d). In addition, we performed Bader charge analysis to verify the charge transfer. The changes of atomic charges of PPy and HPPy upon their introduction on Co(0001) clearly show that the charge transfer is more significantly occurred between Co and N on both PPy-Co(0001) and HPPy-Co(0001) than between Co and other atoms in PPy and HPPy (Fig. S2). This implies that N atoms in PPy and HPPy play a crucial role in the charge depletion of Co surface. This shift is evidence that the electron density was transferred between the loaded Co species and polypyrrole [42]. Such a change in the electronic structure of a metal surface can significantly affect its catalytic property. By electron microscopy method and physical characterization using X-ray, we confirmed that the small Co nanoclusters and polypyrrole chain were uniformly hybridized in Co-PPy-C.

3.2. Electrochemical characterizations

Electrochemical characterization for CO_2RR was conducted in CO_2-saturated 0.1 M $KHCO_3$ solution contained in a cell composed of two-compartment separated by an anion exchange membrane. PPy-C and Co-C (Co-C is a sample for comparison, that was synthesized in the same way for Co-PPy-C, but without polypyrrole.) did not show the catalytic behavior that reduces CO_2 to CO, nor did they produce any other product of CO_2RR, and only HER was observed (Fig. 3a and S3).

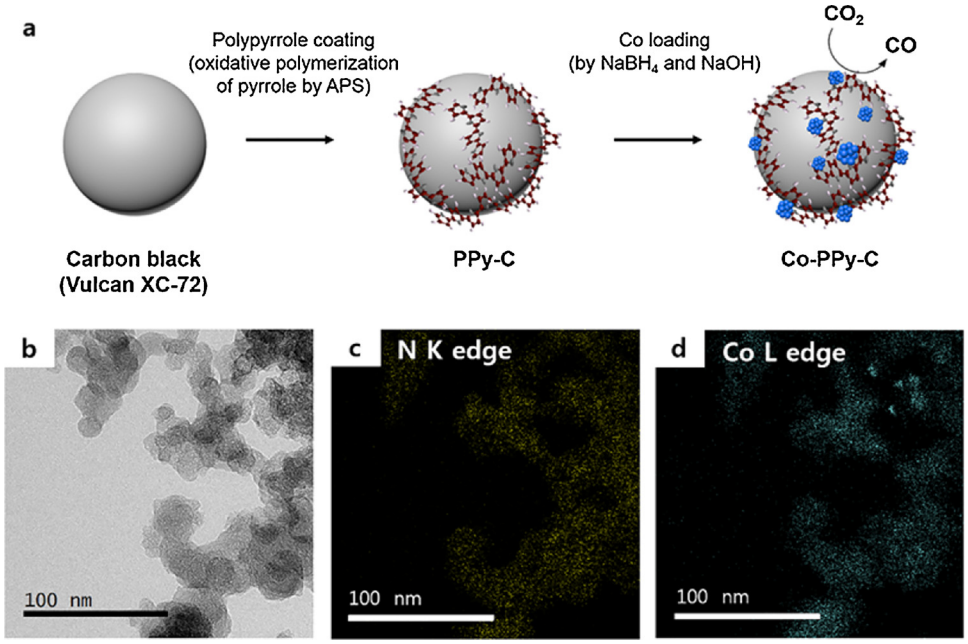

Fig. 1. (a) Schematic description of synthesis of Co-PPy-C. (b) TEM image for Co-PPy-C. (c) N K-edge and (d) Co L-edge EELS mapping images for the same location as Fig. 1b. Yellow spots: N atoms. Blue spots: Co atoms (For interpretation of the references to colour in this figure legend, the reader is referred to the web version of this article).

Meanwhile, Co-PPy-C started to produce CO at 0.45 V vs. RHE (overpotential: 0.35 V). The maximum CO Faradaic efficiency was as high as 78% at 0.55 V, at which overpotential was as low as 0.45 V (Fig. 3a). These results clearly show that the catalytic property of Co-PPy-C to reduce CO_2 to CO is derived from hybridization of Co and polypyrrole. The total faradaic efficiencies of H_2 and CO for the tested samples are presented in Fig. S3. Due to the mass transfer limitation of CO_2 at ambient condition, the CO faradaic efficiency decreased after reaching its maximum. Since Co-PPy-C is more active for CO_2RR than the others, it reached maximum at a relatively lower overpotential. It is noticeable that CO production current of Co-PPy-C normalized by metal (Co) mass was surprisingly high even at the low overpotential region (83 mA

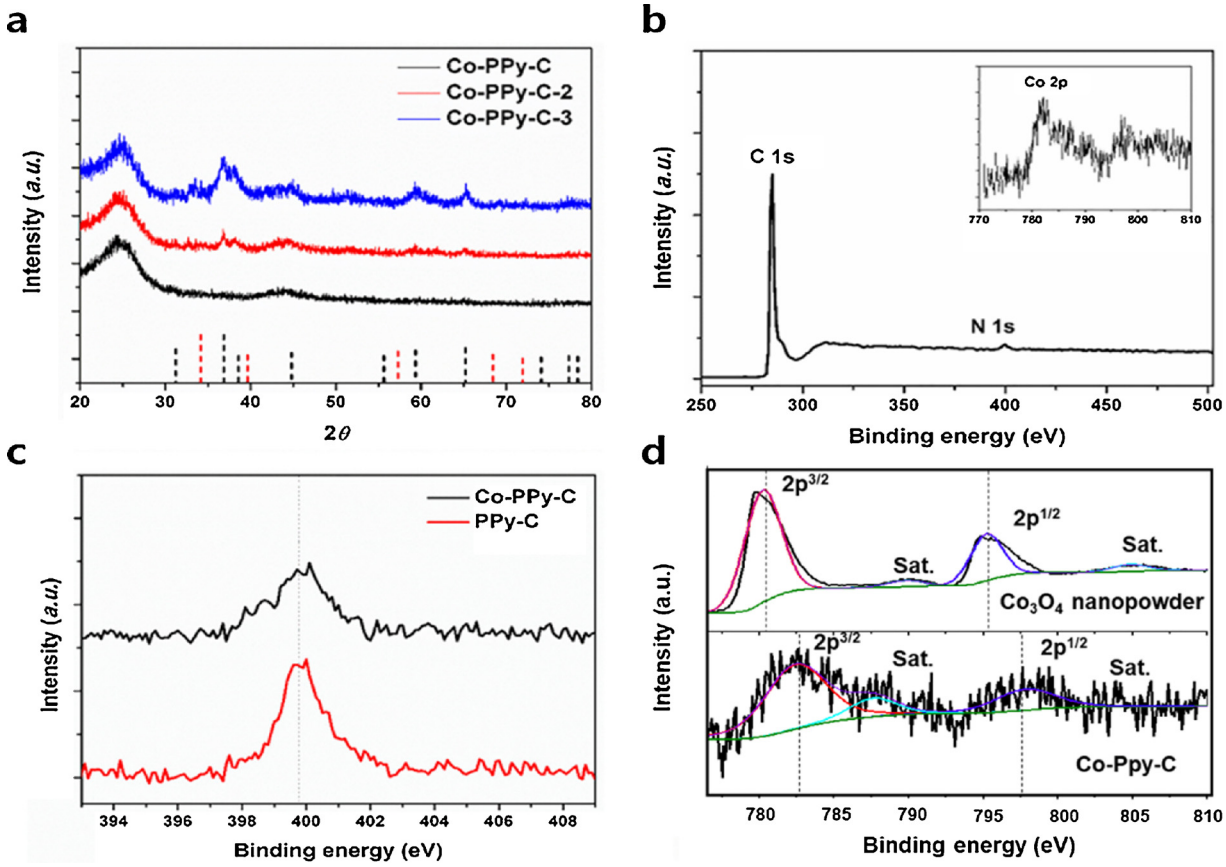

Fig. 2. (a) XRD patterns for Co-PPy-C, Co-PPy-C-2, Co-PPy-C-3, with reference patterns for Co_3O_4 (JCPDS 09-0418) (black dotted vertical lines) and CoO (JCPDS 42-1300) (red dotted vertical lines). (b) XPS elemental survey result for Co-PPy-C. (c) XPS N 1s spectra for Co-PPy-C and PPy-C. (d) XPS Co 2p spectra for Co_3O_4 nanopowder and Co-PPy-C (For interpretation of the references to colour in this figure legend, the reader is referred to the web version of this article).

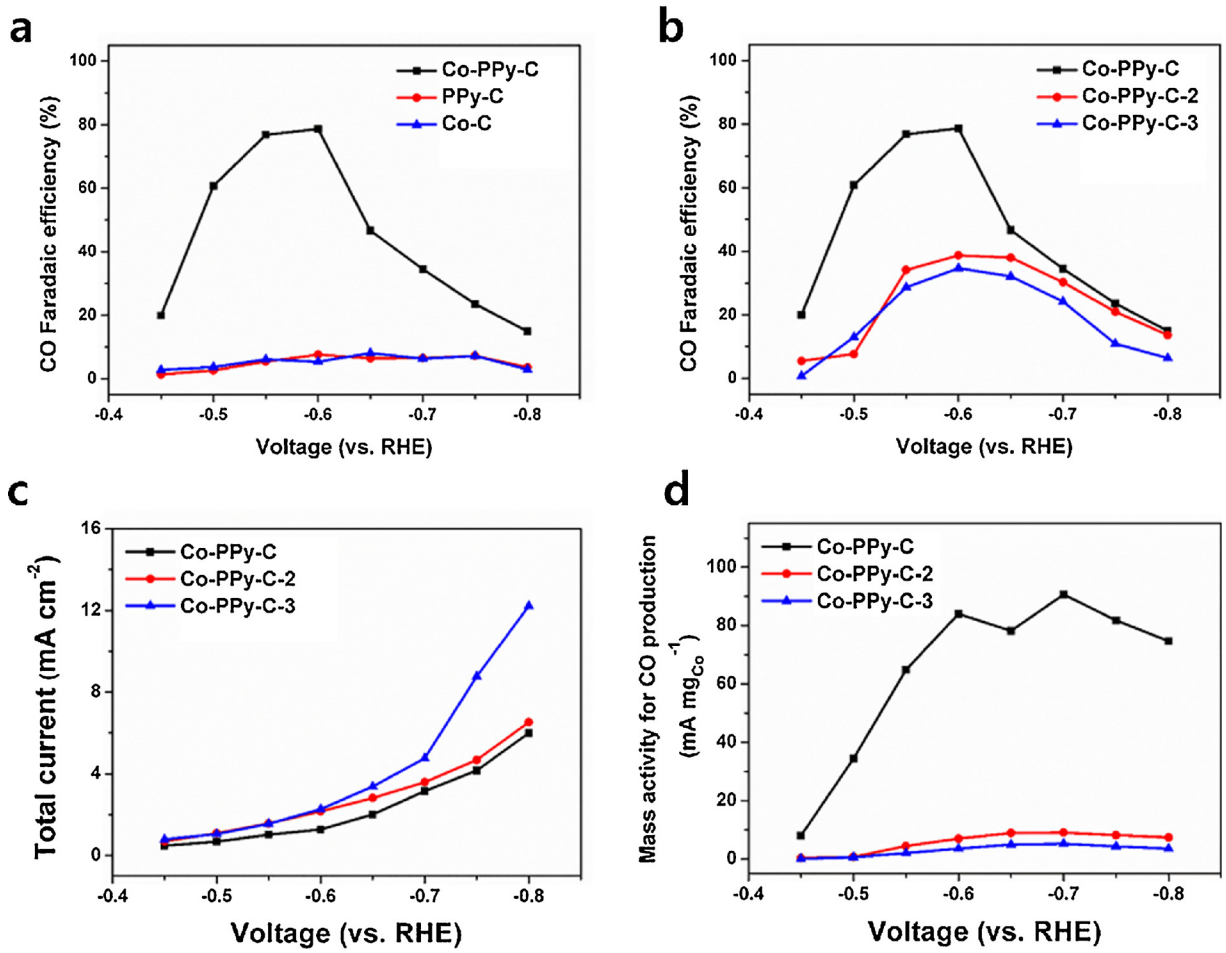

Fig. 3. (a) CO Faradaic efficiencies for Co-PPy-C, PPy-C, and Co-C. (b) CO Faradaic efficiencies, (c) total geometric currents, and (d) CO production currents normalized by Co mass of Co-PPy-C, Co-PPy-C-2, and Co-PPy-C-3.

mg_{Co}^{-1} at 0.55 V; 91 mA mg_{Co}^{-1} at 0.7 V) (Fig. 3d)

Despite the non-nobility of Co, the high mass activity for CO production was comparable to or higher than the highest values obtained using catalysts based on noble-metal nanoparticles (Table S2). The Faradaic efficiency and current for CO production on Co-PPy-C were maintained stable for six hours continuous operation (Fig. S4). Through the ICP measurement, negligible amount of Co dissolution was detected ($\leq$ 25 ppm of Co in Co-PPy-C), which indicated that Co-PPy-C was stable during the electrochemical stability test. These features can enable development of low-cost systems to electrolyze CO_2.

Interestingly, when the amount of Co on PPy-C was increased, the selectivity of CO_2 conversion to CO decreased significantly (Fig. 3b). Co-PPy-C-2 and Co-PPy-C-3 showed maximum CO Faradaic efficiencies of 39% and 35% at 0.6 V, respectively. We attribute this phenomenon to decrease in the effect of polypyrrole on the Co surface. When the amount of Co loaded was increased, large particles ($>$ 10 nm) formed on PPy-C, whereas very small Co nanoclusters ($\sim$ 1 nm) formed uniformly in Co-PPy-C case (Fig. S5). As a result, the portion of the Co surface area that does not contact polypyrrole increased as Co loading was increased, i.e., the portion of catalytic sites generated by contact between Co atoms and polypyrrole decreased, so effective reduction of CO_2 to CO was suppressed. Even if the total currents of Co-PPy-C-2 and Co-PPy-C3 were higher than that of Co-PPy-C (Fig. 3c), the CO production currents per metal mass of the catalysts were much lower than that of Co-PPy-C (Fig. 3d).

3.3. DFT calculations

We performed DFT calculations to elucidate the effect of polypyrrole on the CO_2 reduction at the Co surface. We used a Co (0001) surface to model the Co element in the catalyst. Even though the Co phase in the as-synthesized catalysts is Co_3O_4 as revealed by XRD, the oxide form is reduced to metallic form in a highly-reductive environment in which CO_2 is converted CO on the catalyst in the experiment ($<$ 0.45 V vs. RHE). According to the Pourbaix diagram of Co in the aqueous system, metallic Co is the most stable form below 0.05 V (vs. RHE) when pH is 6.8 (CO_2-saturated 0.1 M $KHCO_3$) [43,44]. The standard reduction potentials of Co^{2+} and Co^{3+} are also much higher than the potentials at which our catalysis was tested [45]. Additionally, we observed that cyclic voltammetry curves of Co-PPy-C and Co_3O_4 nanopowder in N_2-purged 0.1 M $KHCO_3$ solution developed a reduction peak that started to evolve above 0.45 V (vs. RHE), indicating the reduction of Co oxide to metallic Co (Fig. S6).

Pyrrolic functionality in a polypyrrole chain can exist in both protonated form and deprotonated form. Especially, the high reducing potential loaded during CO_2RR can deprotonate pyrrolic N easily [46–48]. Our DFT investigation also revealed that deprotonation reaction energy is very small (0.02 eV/H_{atom}) in the pyrrolic N of polypyrrole, indicating that the deprotonation of N functionality in polypyrrole can occur easily when a strong reducing potential is loaded as our experimental system. We investigated CO_2 reduction on both types of PPy-Co(0001) (deprotonated pyrrolic N) and HPPy-Co(0001) (protonated pyrrolic N) as the model systems of Co-polypyrrole hybrid catalyst.

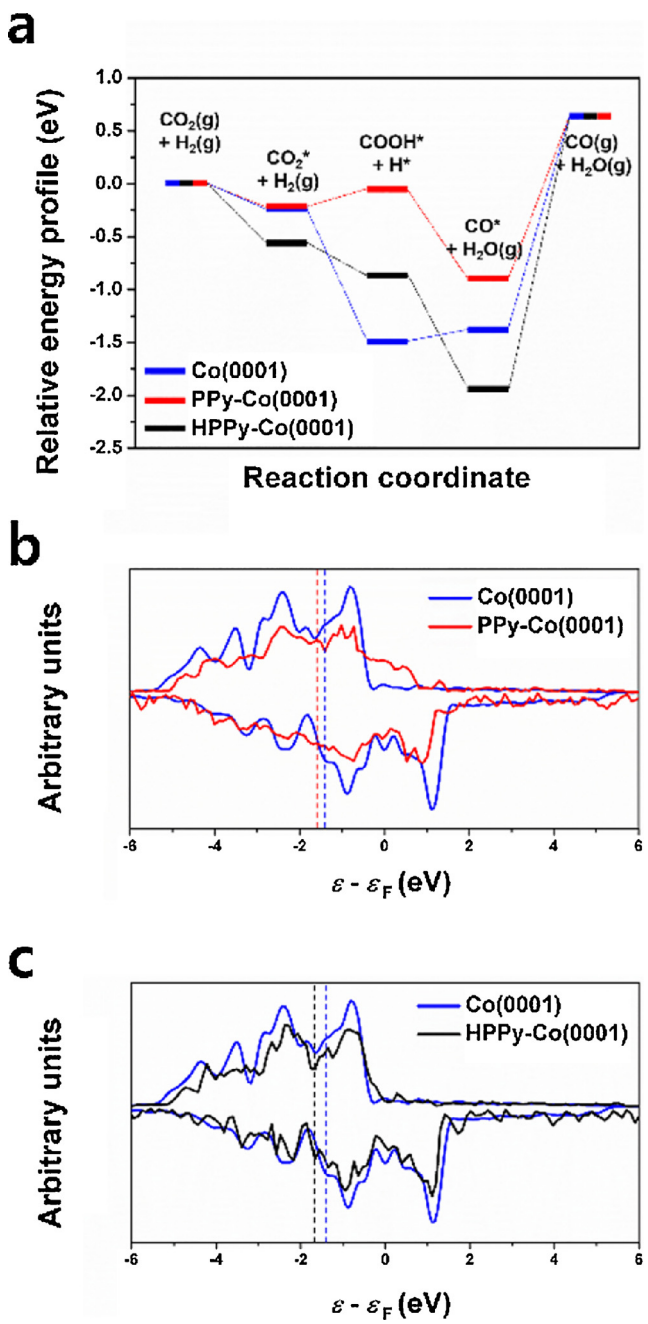

Fig. 4. (a) Relative energy diagram of CO_2RR on Co(0001), PPy-Co(0001), and HPPyCo(0001). Projected density of states (PDOS) of Co 4d states on (b) PPy-Co (0001) and Co(0001); (c) HPPy-Co and Co(0001). The Fermi energy is referenced at E = 0 eV. The dashed vertical lines indicate d-band centers of the surfaces.

Table 1
Adsorption energies (E_{ads}) of CO_2, COOH and CO adsorbed on Co(0001), PPy-Co(0001), and HPPy-Co(0001).

	CO_2	COOH	CO
Co(0001)	−0.24 eV	−3.0 eV	−2.0 eV
PPy-Co(0001)	−0.22 eV	−2.0 eV	−1.5 eV
HPPy-Co(0001)	−0.56 eV	−2.5 eV	−2.6 eV

We adopted a four-step CO_2 reduction mechanism which is widely used to explore CO_2RR (Fig. 4a) [49–51]. The free energy diagram for CO_2 reduction is based on the energetics of molecular adsorption, so we sufficiently examined all possible adsorption sites (Fig. S7) to search for the most preferred active site for molecular adsorption, and obtained optimized structure and adsorption configuration of each state of catalyst surface (Fig. S8). The adsorption energies of the intermediates (Table 1) and the free energy diagram of CO_2RR for CO production (Fig. 4a) indicate that the CO desorption step requires the highest energy in all cases. Because CO is adsorbed on Co surface in all catalyst surfaces (Fig. S8), the overpotential and rate of CO production are changed by the adsorption strength of CO on Co surface. The strongly adsorbed CO slows CO production by blocking the reaction sites. Interestingly, on PPy-Co(0001), the adsorption strength of all intermediates was significantly weakened, and the relative free energy states were also upshifted compared to pure Co(0001) (Table 1; Fig. 4a). In contrast, the adsorption strength of CO was increased when HPPy was introduced to the surface of Co(0001). Based on this result, we suggest that the catalytic site for the selective and fast CO production from CO_2 is a Co surface on which a deprotonated pyrrolic functionality of polypyrrole is adsorbed.

The change of this adsorption property was firstly investigated by calculating the density of states of Co 4d. The d-band structure and energy state of metal surface are closely related to the adsorption property because the molecular orbitals of the adsorbate mainly interact with the d-bands of metal [52]. The d-band centers of Co surfaces in PPy-Co(0001) and HPPy-Co(0001) shown in the density of states are 0.18 eV and 0.22 eV lower than that of Co(0001), respectively. Generally, a downshifted d-band center weakens the interaction between the metal surface and the adsorbate.

The adsorption property of CO_2RR intermediates shown on PPy-Co (0001) is consistent with the general d-band theory, but the change of CO adsorption induced by incorporating HPPy chain on Co(0001) disagrees with the theory. This discrepancy is explained by the further Bader charge analysis (Fig. 5; Table 2). To investigate the origin of enhanced CO adsorption strength on HPPy-Co(0001), we examined the charge transfer from Co surface or (H)PPy to the adsorbed CO. The results showed electron transfers among the Co surface, the adsorbed CO (CO*), and the PPy and HPPy chains. CO molecule is adsorbed preferentially at the sites where the charge depletion occurs due to the pre-adsorbed polymer chains on the Co surface. Those adsorption sites are also close enough for the adsorbates to simultaneously interact with the PPy chain, which is located halfway between N or N-H in the periodic chains of PPy-Co(0001) or HPPy-Co(0001). It has been previously known that charge transfer from metal surface to CO occurs when it is adsorbed on transition metals [53], and that polypyrrole easily donates charges to the adsorbate [38].

The larger charge transfer between Co and CO* induces the stronger adsorption of CO* on Co. When PPy was introduced to the surface of Co (0001), 1.16 e^- electrons were transferred from Co to PPy (Fig. 5). The large depletion of charge on Co surface causes the decrease of electron transfer from Co to CO*, so the interaction between Co and CO* weakens. In contrast, HPPy chain withdraws much less electrons from Co surface (0.64 e^-), and donates more electrons to CO* than does PPy chain (Table 2). As a result, CO* takes larger charge density from the Co surface in HPPy-Co(0001) than from the Co surface in Co(0001), so CO* is more stable on HPPy-Co(0001) than on Co(0001), even though the d-band center is lower in HPPy-Co(0001) than in Co(0001). Although the adsorption property observed on HPPy-Co(0001) is not advantageous to the catalysis for CO_2RR, this observation may provide a clue to break the scaling relationship that limits the activity of metal catalyst, in that the adsorption strength of each intermediates is independently controlled.

4. Conclusions

Metal-organic hybrid material of Co and polypyrrole showed a high electrocatalytic activity for CO production by CO_2RR, even though Co and polypyrrole individually do not have catalytic property to convert

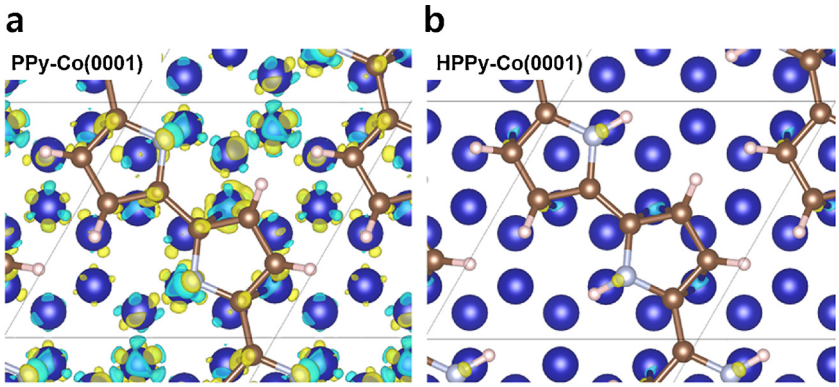

Fig. 5. Charge density difference plots obtained by Bader charge analysis upon the introduction of (a) PPy and (b) HPPy onto the Co(0001) surface with an isosurface value of 0.0015 e $bohr^{-3}$. Yellow region: electron rich; cyan region: electron depletion (For interpretation of the references to colour in this figure legend, the reader is referred to the web version of this article).

Table 2
Electron transfer on each catalyst surface obtained by Bader charge upon CO adsorption.

Catalyst surface	Transfer direction	Transferred charge
Co(0001)	Co → CO*	0.43 e^-
PPy-Co(0001)	Co → CO*	0.33 e^-
	PPy → CO*	0.12 e^-
HPPy-Co(0001)	Co → CO*	0.52 e^-
	HPPy → CO*	0.24 e^-

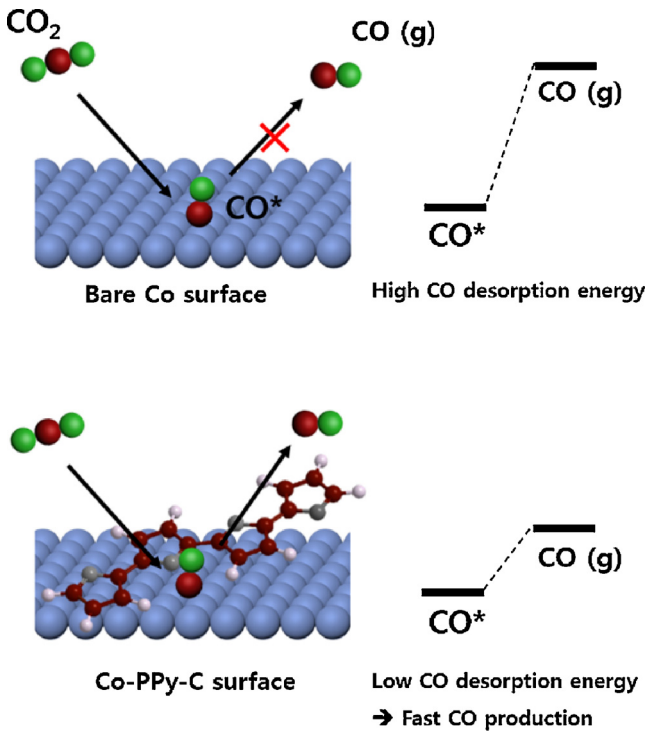

Fig. 6. Difference of CO_2RR on bare Co surface and Co-PPy-C surface.

CO_2 to CO. The selectivity for CO production was high even at the low overpotential region, and the metal mass activity was one of the highest that has been reported for catalysts based on metal particles. This highly selective and fast CO production by CO_2RR on non-noble metal catalyst in aqueous phase is a noteworthy phenomenon. Our DFT calculations revealed that the modified electrocatalysis of Co surface for CO_2RR was due to the decrease of adsorption strength of CO on Co as a result of the significant charge transfer between Co surface and polypyrrole chain (Fig. 6). This work does not only report the new CO_2RR catalyst material and its catalytic behavior, but also suggests that hybridization of metal and organic material can be a useful strategy to overcome the current limitations of metal catalysts for CO_2RR.

Acknowledgement

This work was supported by the Samsung Research Funding center of Samsung Electronics under Project Number SRFC-MA1601-05 and SRFC-MA1402-14.

Appendix A. Supplementary data

Supplementary material related to this article can be found, in the online version, at doi:https://doi.org/10.1016/j.apcatb.2018.05.025.

References

[1] S.H. Schneider, The greenhouse effect: science and policy, Science 243 (1989) 771–781.
[2] M.S. Dresselhaus, I.L. Thomas, Alternative energy technologies, Nature 414 (2001) 332–337.
[3] D. Larcher, J.M. Tarascon, Towards greener and more sustainable batteries for electrical energy storage, Nat. Chem. 7 (2015) 19–29.
[4] G. Centi, E.A. Quadrelli, S. Perathoner, Catalysis for CO2 conversion: a key technology for rapid introduction of renewable energy in the value chain of chemical industries, Energy Environ. Sci. 6 (2013) 1711–1731.
[5] J. Albo, A. Sáez, J. Solla-Gullón, V. Montiel, A. Irabien, Production of methanol from CO2 electroreduction at Cu2O and Cu2O/ZnO-based electrodes in aqueous solution, Appl. Catal. B 176 (2015) 709–717.
[6] D.T. Whipple, P.J.A. Kenis, Prospects of CO2 utilization via direct heterogeneous electrochemical reduction, J. Phys. Chem. Lett. 1 (2010) 3451–3458.
[7] D.D. Zhu, J.L. Liu, S.Z. Qiao, Recent advances in inorganic heterogeneous electrocatalysts for reduction of carbon dioxide, Adv. Mater. 28 (2016) 3423–3452.
[8] N. Gutierrez-Guerra, L. Moreno-Lopez, J.C. Serrano-Ruiz, J.L. Valverde, A. de Lucas-Consuegra, Gas phase electrocatalytic conversion of CO2 to syn-fuels on Cu based catalysts-electrodes, Appl. Catal. B 188 (2016) 272–282.
[9] J.H. Kim, H. Woo, S.W. Yun, H.W. Jung, S. Back, Y. Jung, Y.T. Kim, Highly active and selective Au thin layer on Cu polycrystalline surface prepared by galvanic displacement for the electrochemical reduction of CO2 to CO, Appl. Catal. B 213 (2017) 211–215.
[10] M.S. Jee, H.S. Jeon, C. Kim, H. Lee, J.H. Koh, J. Cho, B.K. Min, Y.J. Hwang, Enhancement in carbon dioxide activity and stability on nanostructured silver electrode and the role of oxygen, Appl. Catal. B 180 (2016) 372–378.
[11] T. Bligaard, J.K. Nørskov, S. Dahl, J. Matthiesen, C.H. Christensen, J. Sehested, The Brønsted–Evans–Polanyi relation and the volcano curve in heterogeneous catalysis, J. Catal. 224 (2004) 206–217.
[12] H.A. Hansen, J.B. Varley, A.A. Peterson, J.K. Nørskov, Understanding trends in the electrocatalytic activity of metals and enzymes for CO2 reduction to CO, J. Phys. Chem. Lett. 4 (2013) 388–392.
[13] Y. Hori, Electrochemical CO2 reduction on metal electrodes, in: C.G. Vayenas, R.E. White, M.E. Gamboa-Aldeco (Eds.), Modern Aspects of Electrochemistry, Springer New York, New York, NY, 2008, pp. 89–189.
[14] S. Uhm, Y.D. Kim, Electrochemical conversion of carbon dioxide in a solid oxide electrolysis cell, Curr. Appl. Phys. 14 (2014) 672–679.
[15] A.S. Agarwal, Y. Zhai, D. Hill, N. Sridhar, The electrochemical reduction of carbon dioxide to formate/formic acid: engineering and economic feasibility, ChemSusChem 4 (2011) 1301–1310.
[16] E. Iglesia, Design, synthesis, and use of cobalt-based Fischer-Tropsch synthesis catalysts, Appl. Catal. A 161 (1997) 59–78.
[17] Q. Lu, J. Rosen, Y. Zhou, G.S. Hutchings, Y.C. Kimmel, J.G. Chen, F. Jiao, A selective and efficient electrocatalyst for carbon dioxide reduction, Nat. Commun. 5 (2014) 3242.
[18] N. Yoneda, S. Kusano, M. Yasui, P. Pujado, S. Wilcher, Recent advances in processes

and catalysts for the production of acetic acid, Appl. Catal. A 221 (2001) 253–265.
[19] H.-M. Koo, G.Y. Han, J.W. Bae, Fischer-Tropsch synthesis on the cobalt impregnated catalyst using carbon-coated Ni/SiO2, Korean J. Chem. Eng. 33 (2016) 1565–1570.
[20] D. Gao, H. Zhou, J. Wang, S. Miao, F. Yang, G. Wang, J. Wang, X. Bao, Size-Dependent electrocatalytic reduction of CO2 over Pd nanoparticles, J. Am. Chem. Soc. 137 (2015) 4288–4291.
[21] C. Kim, H.S. Jeon, T. Eom, M.S. Jee, H. Kim, C.M. Friend, B.K. Min, Y.J. Hwang, Achieving selective and efficient electrocatalytic activity for CO2 reduction using immobilized silver nanoparticles, J. Am. Chem. Soc. 137 (2015) 13844–13850.
[22] W. Zhu, R. Michalsky, Ö. Metin, H. Lv, S. Guo, C.J. Wright, X. Sun, A.A. Peterson, S. Sun, Monodisperse Au nanoparticles for selective electrocatalytic reduction of CO2 to CO, J. Am. Chem. Soc. 135 (2013) 16833–16836.
[23] Y.S. Ham, S. Choe, M.J. Kim, T. Lim, S.-K. Kim, J.J. Kim, Electrodeposited Ag catalysts for the electrochemical reduction of CO2 to CO, Appl. Catal. B 208 (2017) 35–43.
[24] M. Asadi, B. Kumar, A. Behranginia, B.A. Rosen, A. Baskin, N. Repnin, D. Pisasale, P. Phillips, W. Zhu, R. Haasch, R.F. Klie, P. Král, J. Abiade, A. Salehi-Khojin, Robust carbon dioxide reduction on molybdenum disulphide edges, Nat. Commun. 5 (2014) 4470.
[25] B. Kumar, M. Asadi, D. Pisasale, S. Sinha-Ray, B.A. Rosen, R. Haasch, J. Abiade, A.L. Yarin, A. Salehi-Khojin, Renewable and metal-free carbon nanofibre catalysts for carbon dioxide reduction, Nat. Commun. 4 (2013) 2819.
[26] J.K. Norsko, Chemisorption on metal surfaces, Rep. Prog. Phys. 53 (1990) 1253.
[27] H.A. Hansen, C. Shi, A.C. Lausche, A.A. Peterson, J.K. Norskov, Bifunctional alloys for the electroreduction of CO2 and CO, Phys. Chem. Chem. Phys. 18 (2016) 9194–9201.
[28] P. Sabatier, Hydrogénations et déshydrogénations par catalyse, Ber. Dtsch. Chem. Ges. 44 (1911) 1984–2001.
[29] A.A. Peterson, J.K. Nørskov, Activity descriptors for CO2 electroreduction to methane on transition-metal catalysts, J. Phys. Chem. Lett. 3 (2012) 251–258.
[30] H.-K. Lim, H. Shin, W.A. Goddard, Y.J. Hwang, B.K. Min, H. Kim, Embedding covalency into metal catalysts for efficient electrochemical conversion of CO2, J. Am. Chem. Soc. 136 (2014) 11355–11361.
[31] K. Lee, L. Zhang, H. Lui, R. Hui, Z. Shi, J. Zhang, Oxygen reduction reaction (ORR) catalyzed by carbon-supported cobalt polypyrrole (Co-PPy/C) electrocatalysts, Electrochim. Acta 54 (2009) 4704–4711.
[32] R. Bashyam, P. Zelenay, A class of non-precious metal composite catalysts for fuel cells, Nature 443 (2006) 63–66.
[33] D. Sholl, J. Steckel, Density Functional Theory: a Practical Introduction, 2009, John Wiley and Sons, Hoboken, 2009.
[34] G. Kresse, J. Furthmüller, Efficient iterative schemes for ab initio total-energy calculations using a plane-wave basis set, Phys. Rev. B 54 (1996) 11169–11186.
[35] J.P. Perdew, K. Burke, M. Ernzerhof, Generalized gradient approximation made simple, Phys. Rev. Lett. 77 (1996) 3865–3868.
[36] H.J. Monkhorst, J.D. Pack, Special points for brillouin-zone integrations, Phys. Rev. B 13 (1976) 5188–5192.
[37] M. Hömberg, M. Müller, Main phase transition in lipid bilayers: phase coexistence and line tension in a soft, solvent-free, coarse-grained model, J. Chem. Phys. 132 (2010) 155104.
[38] D.-G. Lee, S.H. Kim, S.H. Joo, H.-I. Ji, H. Tavassol, Y. Jeon, S. Choi, M.-H. Lee, C. Kim, S.K. Kwak, G. Kim, H.-K. Song, Polypyrrole-assisted oxygen electrocatalysis on perovskite oxides, Energy Environ. Sci. 10 (2017) 523–527.
[39] O. Knacke, O. Kubaschewski, K. Hesselmann, Thermochemical Properties of Inorganic Substances, Springer, Berlin, 1991.
[40] M. Żyła, G. Smoła, A. Knapik, J. Rysz, M. Sitarz, Z. Grzesik, The formation of the Co3O4 cobalt oxide within CoO substrate, Corros. Sci. 112 (2016) 536–541.
[41] R. Liu, D. Wu, X. Feng, K. Müllen, Nitrogen-doped ordered mesoporous graphitic arrays with high electrocatalytic activity for oxygen reduction, Angew. Chem. Int. Ed. 49 (2010) 2565–2569.
[42] S. Porsgaard, P. Jiang, F. Borondics, S. Wendt, Z. Liu, H. Bluhm, F. Besenbacher, M. Salmeron, Charge state of gold nanoparticles supported on titania under oxygen pressure, Angew. Chem. Int. Ed. 50 (2011) 2266–2269.
[43] M. Pourbaix, Atlas of Electrochemical Equilibria in Aqueous Solutions, National Association of Corrosion Engineers, (1974).
[44] L.G. Bloor, P.I. Molina, M.D. Symes, L. Cronin, Low pH electrolytic water splitting using earth-abundant metastable catalysts that self-assemble in situ, J. Am. Chem. Soc. 136 (2014) 3304–3311.
[45] W.M. Haynes, CRC Handbook of Chemistry and Physics, CRC press, 2014.
[46] N.V. Blinova, J. Stejskal, M. Trchová, J. Prokeš, M. Omastová, Polyaniline and polypyrrole: a comparative study of the preparation, Eur. Polym. J. 43 (2007) 2331–2341.
[47] D.Y. Kim, J.Y. Lee, D.K. Moon, C.Y. Kim, Stability of reduced polypyrrole, Syn. Met. 69 (1995) 471–474.
[48] J. Skodova, D. Kopecky, M. Vrnata, M. Varga, J. Prokes, M. Cieslar, P. Bober, J. Stejskal, Polypyrrole-silver composites prepared by the reduction of silver ions with polypyrrole nanotubes, Polym. Chem. 4 (2013) 3610–3616.
[49] M. Li, J. Wang, P. Li, K. Chang, C. Li, T. Wang, B. Jiang, H. Zhang, H. Liu, Y. Yamauchi, N. Umezawa, J. Ye, Mesoporous palladium-copper bimetallic electrodes for selective electrocatalytic reduction of aqueous CO2 to CO, J. Mater. Chem. A 4 (2016) 4776–4782.
[50] C. Liu, H. He, P. Zapol, L.A. Curtiss, Computational studies of electrochemical CO2 reduction on subnanometer transition metal clusters, Phys. Chem. Chem. Phys. 16 (2014) 26584–26599.
[51] Y. Liu, J. Zhao, Q. Cai, Pyrrolic-nitrogen doped graphene: a metal-free electrocatalyst with high efficiency and selectivity for the reduction of carbon dioxide to formic acid: a computational study, Phys. Chem. Chem. Phys. 18 (2016) 5491–5498.
[52] B. Hammer, J.K. Nørskov, Theoretical surface science and catalysis—calculations and concepts, Adv. Catal. 45 (2000) 71–129.
[53] M. Gajdoš, A. Eichler, J. Hafner, CO adsorption on close-packed transition and noble metal surfaces: trends from ab initio calculations, J. Phys. Condens. Matter 16 (2004) 1141.